UAB LIBRARIES
The University of Alabama at Birmingham

Inquiro, the UAB undergraduate science research journal

Volume 2012 | Number 6 Article 19

2012

Design of a Torsion Tester for Study of the Effects of Diabetes and Obesity on Murine Bone Properties

Brandon Sherrod

Shawn Gilbert

Krista Casazza

Alan Eberhardt

Follow this and additional works at: https://digitalcommons.library.uab.edu/inquiro

 Part of the Higher Education Commons

Recommended Citation

Sherrod, Brandon; Gilbert, Shawn; Casazza, Krista; and Eberhardt, Alan (2012) "Design of a Torsion Tester for Study of the Effects of Diabetes and Obesity on Murine Bone Properties," *Inquiro, the UAB undergraduate science research journal*: Vol. 2012: No. 6, Article 19.
Available at: https://digitalcommons.library.uab.edu/inquiro/vol2012/iss6/19

This content has been accepted for inclusion by an authorized administrator of the UAB Digital Commons, and is provided as a free open access item. All inquiries regarding this item or the UAB Digital Commons should be directed to the UAB Libraries Office of Scholarly Communication.

research paper

Design of a Torsion Tester for Study of the Effects of Diabetes and Obesity on Murine Bone Properties

Brandon Sherrod[1], Shawn Gilbert[2], Krista Casazza[3], and Alan Eberhardt[1]
[1] Department of Biomedical Engineering, [2] Department of Orthopaedic Surgery, [3] Department of Nutrition Sciences, University of Alabama at Birmingham

Abstract

Characterization of bone mechanical integrity is critical when assessing effects of orthopedic surgical procedures and conditions such as diabetes and obesity. Since long bones experience torsional loading *in vivo*, mechanical characterization of torsional loading *in vitro* is a critical step in assessing the integrity of bone. Prior to this project, UAB's testing facilities did not possess the capability to perform torsional testing on bone. The goal of this research effort was to design a cost-effective mechanism for translating the linear motion of the available testing equipment into rotational motion for torsional loading of murine (mouse) bone until failure. After successful development of the apparatus for testing, 9 (n=9) femurs from 3 age groups of non-obese diabetic-resistant (NOR) female mice were torqued at a rate of one degree per second until failure was observed in the diaphyseal region of the femora. Maximum torque, maximum shear stress, and torsional rigidity were calculated from test results. Micro-computed tomography (μCT) and bright field microscopy imaging were performed on the bone specimens. Age, femoral length, and bone density were all positively and significantly ($p < 0.05$) correlated with torsional strength. Values for maximum torque at 73 days of age were similar to values determined in previous studies on torsional loading of murine bone. Future studies will further investigate the relationships between previously mentioned conditions and bone mechanical integrity.

Introduction

Factors affecting bone strength include age, bone geometry (e.g. length, cross-sectional area, area moment of inertia, and thickness), species of origin, density, bone volume fraction, and cumulative effects (fatigue effects) of loads sustained over a lifetime [1,2]. Diseases and certain surgical procedures can also affect the strength of bone. Obesity and diabetes have both been associated with alterations in bone structure and strength. Diabetes has been associated with deterioration of bone integrity [3], and obesity with adverse alterations in bone metabolism [4] and mechanical integrity [5]. Studies have shown that diabetic rodent models exhibit lower levels of new bone formation during fracture healing [6], lower bone mineral density (BMD) [7], and increased risk of fracture [3]. There are differences, however, in the integrity of bone samples from type I and type II diabetics. These differences are most likely due to obesity [7].

Findings from research on obesity's effects on bone integrity have been controversial. Although there is an increase in bone mineral density (BMD) with increasing body mass index (BMI) and a decrease in fracture incidence in the central body regions of obese women compared to those of healthy weight women due to soft tissue padding, there is an increase in fracture incidence in the extremities [8]. Other studies have shown that while cortical bone strength may not be adversely affected by high-fat diets, cancellous BMD and mechanical strength were significantly lower in mice with high-fat diets than in mice with low-fat diets [9]. In addition, extreme obesity has been associated with lower BMD despite the general trend of increased BMD with higher BMI [10]. Researchers at UAB are particularly interested in assessing the mechanical integrity of bone specimens of mice with diabetes and high-fat diets to determine if obesity or diabetes is associated with decreased or increased mechanical integrity of murine long bones.

Orthopedic surgeons are also interested in assessing the strength of murine long bones following use of methods that increase the rate of post-operation healing for a limb lengthening procedure known as distraction osteogenesis (DO). The DO procedure utilizes fracture healing of bone, a physiologically unique process that produces a regenerative callous at the fracture site. This callous will grow to fill the gap created by the fracture. Normal physiological fractures can be caused by loads exceeding the strength of bone, pathological weakening of bone, or fatigue fractures [1]. In the case of DO and limb lengthening, the fracture is created intentionally during surgery by removal of a portion of the diaphyseal region of the long bone by corticotomy. UAB researchers are interested in alterations of hypoxia-inducing pathways that have been found to accelerate the post-surgery healing process in animal models [11]. However, mechanical validation of the integrity of treated bone specimens has not been performed.

Spiral fractures are the result of torsional loading about the longitudinal axis of the whole bone. For example, a tibial fracture can often be explained by a force couple that results from the shear and frictional forces between the foot and the ground [12]. Fatigue fractures, or stress fractures, that result from torsional loading can be more easily induced than stress fractures caused by compressive or tensile loading [12,13]. The shear stress experienced by the bone in torsion is distributed over the entire bone structure (in the parallel and perpendicular

planes to the neutral axis), whereas the maximum tensile and compressive stresses occur in the plane diagonal to the neutral axis [14]. Because torsion results in shear, compressive, and tensile forces, it is an ideal *in vitro* loading test to assess the mechanical integrity of a long bone specimen. Because torsional loading is applied to the ends of whole bones, this loading pattern is applied away from defects and the site of fracture healing for fractures in the diaphysis. Torsional loading is therefore an important experimental loading mode in studies on fracture healing and DO, which is performed in the diaphysis of long bones rather than the ends.

The applied torque experienced in torsional loading can be characterized mathematically using the following equation:

$$T=Fd$$

where T is applied torque, F is applied axial force, and d is length of the moment arm. In this experiment, F is the negative force that the load cell measures as the pinion gear resists the twisting motion, and d is the distance from the rack gear to the center of the bone specimen, which is the pitch radius of the pinion gear. If T can be calculated as described above, then the maximum shear stress, which will occur at the outer edge of the bone specimen, can be calculated using the following equation:

$$\tau=Tr / J$$

where τ is shear stress, T is applied torque, r is the radius of the bone specimen, and J is polar moment of inertia (analogous to area moment of inertia). The polar moment of inertia and specimen radius are found using micro-computed tomography (μCT) scans (see methods section). The torsional stiffness of the specimen is calculated based on the slope of the torque versus angular displacement curve (T vs. θ curve):

$$K= \Delta T / \Delta\theta$$

where K is torsional stiffness, T is applied torque, and θ is angular displacement. Many of the calculations for torque and torsional shear stress result in a high error rate [15]; however, this error can be mitigated by using μCT scans rather than manual measurements to obtain geometrical parameters.

Prior to this project, UAB's testing facilities did not possess the capability to perform torsional testing on bone. The goal of this research effort was to design a cost-effective mechanism for translating the linear motion of the available testing equipment into rotational motion for torsional loading of murine bone until failure. A torsional testing system was designed that is capable of applying a range of torques from 0 to 265 N • mm to a rodent long bone specimen. Nine (n=9) murine femur specimens from non-obese diabetic resistant (NOR) mice of different ages were tested in torsional loading after μCT scans were performed to assess geometrical properties and bone densities of the femora. It was hypothesized that, if the device design was effective, there would be a significant and positive correlation between torsional strength and femoral length, geometry (i.e. radius and polar moment of inertia), age, and density. The results should also be relatively similar to results from previous studies on mechanical testing on murine long bones in torsion.

Materials and Methods

Device Design

Three goals guided the design of the torsion testing apparatus: translate the linear motion of the available lab equipment into rotational motion, use a cost-effective design, and keep the construction simple and accessible.

A rack and pinion gear system (Figure 1A) was initially modeled in PTC Creo® 3D software to attain a basic grasp of the feasibility of such a system. Due to design constraints such as cost, space, machining equipment limitations, and specimen size, the simplified rack and pinion system was determined to be feasible. A more detailed computer-aided design (CAD) model of the rack and pinion system with additional components was constructed (Figure 1B and 1C) as a more accurate representation of the testing system scale. The components of the assembly were ordered from various manufacturers (see Appendix A2) in a manner that would minimize cost. Machining was performed as necessary on the lathe, drill press, mill, and bandsaw. The aluminum gearshaft was turned on the lathe to decrease the diameter of the gear attachment end to 0.125 inches. The outer and inner aluminum tubings were cut with the bandsaw to a length of one inch each. A free body diagram was constructed (Figure 2) to visualize the force vectors and resultant torque on the bone specimen upon axial loading by the rack gear.

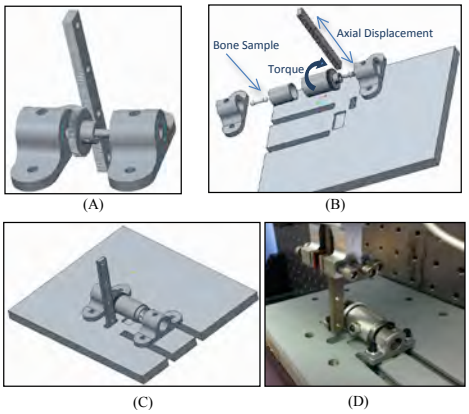

Figure 1. Apparatus design and components. (A) Initial rack and pinion gear concept. (B) Exploded view of components. (C) Final CAD assembly. (D) Final assembly on testing platform.

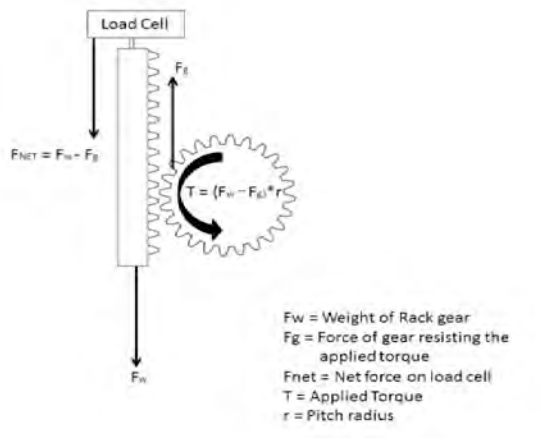

Figure 2. Free body diagram of the rack gear, pinion gear, and load cell.

Experimental Procedure

Murine femur samples were obtained from the lab of Dr. Krista Casazza in the UAB Webb Nutritional Sciences Building. Samples were frozen in phosphate buffered saline (PBS) solution during storage. Micro-computed tomography (μCT) scans were performed on each femur specimen with a Scanco Medical (Brüttisellen, Switzerland) μCT 40 scanner. Each specimen was scanned to obtain 25 slices (equivalent to a 0.3 mm thick section) of the mid diaphysis. Values obtained from the μCT scans included specimen length, bone density, polar moment of inertia, bone volume, and outer radius.

Prior to torsional testing, the bone specimens were trimmed of excess connective tissue and allowed to thaw in PBS solution for 15 minutes by wrapping the specimen in a saline-saturated towelette. Poly-methyl methacrylate (PMMA) bone cement was prepared using 2 parts PMMA powder and 1 part monomer liquid. The proximal end of the femur was potted in the center of the inner rotating tubing using PMMA bone cement, and the distal end was potted in the center of the stationary block housing using PMMA cement. Once the cement had sufficiently hardened, the entire device (Figure 1D) was set on the Bose Electroforce® LM1 Testing System (Eden Prairie, Minnesota) platform. The rack gear was connected to the load cell using an adapter attachment. The load cell has a maximum loading capacity of five pounds, or approximately 265 N • mm of torque with an 11.906 mm moment arm. The femur specimens were loaded in axial torsion until failure at a rate of one degree per second [16,17], requiring the linear displacement rate of the rack gear to be 0.2072 millimeters per second (see Appendix A1). Spiral fracture was observed in the diaphyseal region of the mouse femora (Figure 4A). Torque was calculated by multiplying the applied force on the pinion gear by the pitch radius of the gear, which is 11.906 mm. Data were collected at a rate of 136 Hz. Post-testing imaging was performed on a Nikon SMZ 3000 Microscope optics system using SPOT image acquisition software and equipment to obtain Figure 4C-E.

Statistical Analysis

Three hypotheses were formulated to validate the efficacy of the design: femoral length will affect the maximum torque required to induce failure; age of the mouse will affect the maximum torque required to induce failure; and bone density will affect the maximum torque required to induce failure. Statistical analyses were conducted using one-way ANOVA tests and linear regression. Significance was set at 95% confidence ($p < 0.05$). A total of nine (n=9) femurs were tested in torsion. Each age group of femurs (46 days, 62 days, 73 days) had 3 specimens (n=3) per group.

Results

Data from the torsional testing until failure and μCT imaging analysis of femurs from NOR (non-obese diabetic resistant) mice are displayed in Table 1. Bone density, polar moment of inertia, and outer radius were found by taking the mean values from 25 CT slices taken at the middle of the diaphysis. A 25-slice section is 0.3 mm thick. HA refers to hydroxyapatite. Table 2 displays mean values for maximum torque at failure, maximum shear stress, and torsional stiffness for each age group of NOR mice. Figure 3 displays linear regression plots of maximum torque versus femoral length (Figure 3A) and of maximum torque versus bone density (Figure 3B). Figure 4 displays post-testing images of spiral fracture observed in the femur specimens along with a CT scan construction of the middle portion of the diaphysis.

Table 1. Age, Femoral Length, Bone Density, Polar MOI, and Outer Radius Measurements for NOR mice (means ± standard deviation)

Age (days)	n	Specimen Length (mm)	Bone Density (mg HA/cm^3)	Polar Moment of Inertia (mm^4)	Outer Radius (mm)
46	3	11.26 ± 1.14	1262.252 ± 24.336	0.149 ± 0.016	0.639 ± 0.012
62	3	14.08 ± 0.53	1338.155 ± 6.485	0.208 ± 0.021	0.682 ± 0.035
73	3	14.29 ± 0.35	1376.493 ± 22.310	0.216 ± 0.010	0.690 ± 0.011

Table 2. Results from Torsional Loading Until Failure Tests (means ± standard deviation)

Age (days)	n	Maximum Torque at Failure (N • mm)	Max Shear Stress (MPa)	Torsional Stiffness (N • mm/degree)
46	3	10.42 ± 0.47	44.93± 4.39	0.419 ± 0.034
62	3	15.66 ± 1.76	51.31 ± 4.66	0.749 ± 0.139
73	3	17.26 ± 1.37	55.31 ± 5.11	0.903 ± 0.281

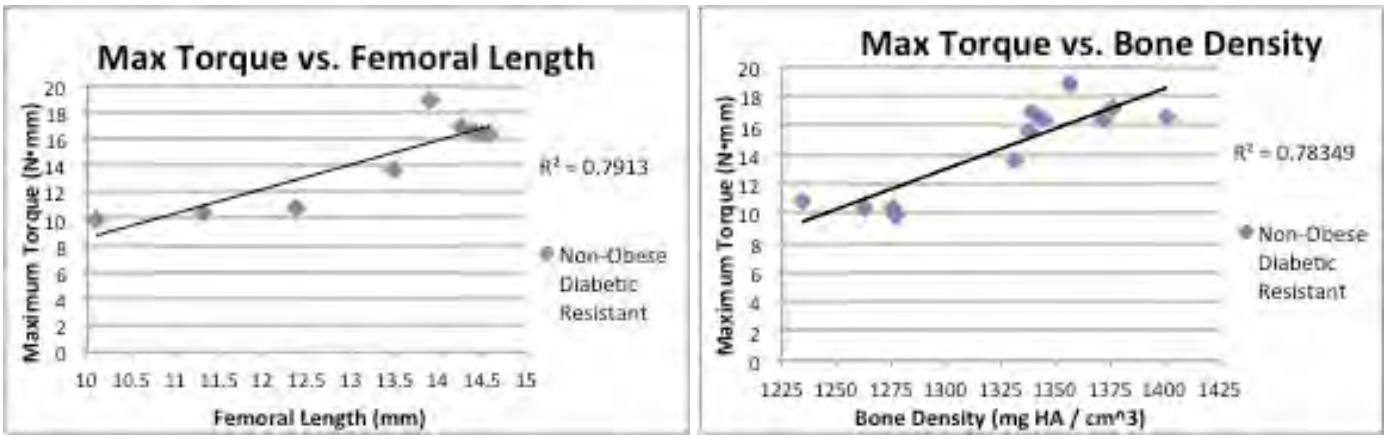

A B

Figure 3. Linear regression plots of Max Torque vs. Specimen Length (A) and Max Torque vs. Bone Density (B)

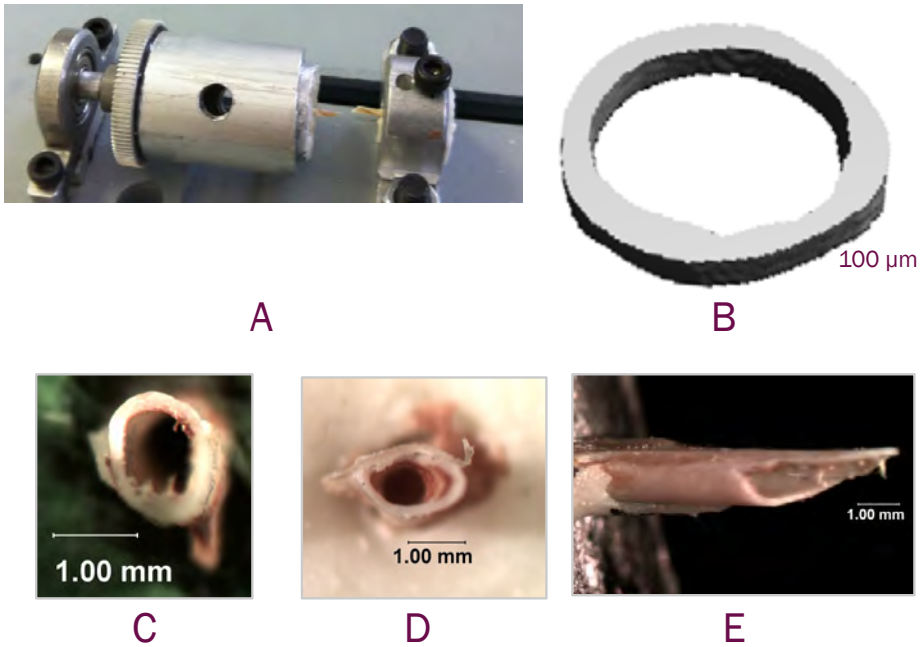

A B C D E

Figure 4. (A) Apparatus containing a potted femur specimen post-fracture. (B) A µCT scan image of the 25 compiled slices from the mid-diaphysis. (C,D) Axial images of cross-sectional view of fracture. (E) Lateral view of spiral fracture.

Results for hypothesis testing by statistical analysis are discussed below. Hypotheses are stated and numbered with respective results. Tests were performed using one-way ANOVA via linear regression analysis.

1) Hypothesis 1: Femoral length affects maximum torque required to induce failure. The dependent variable was torque, and the independent variable was the femoral length.
Results: p-value for probability of null hypothesis was found to be 0.0021 ($p < 0.05$). The F-test statistic was found to be 26.682. Linear regression analysis shows a positive correlation between femoral length and maximum torque with a correlation coefficient of 0.8895 and an R^2 value of 0.7913.

2) Hypothesis 2: Specimen age affects maximum torque required to induce specimen failure.
Results: p-value for probability of null hypothesis was found to be 0.0017 ($p < 0.05$). The F-test statistic was found to be 22.19. Additionally, the average maximum torque increased 65.6% from 46 day old specimens to 73 day old specimens.

3) Hypothesis 3: Bone density affects maximum torque required to induce specimen failure.
Results: p-value for probability of the null hypothesis was found to be 0.0079 ($p < 0.05$). The F-test statistic was found to be 15.231. Linear regression analysis showed a positive correlation between bone density and maximum torque with a correlation coefficient of 0.8529 and an R^2 value of 0.7835.

Discussion

The results indicate that the factors of age, femoral length, and bone density are all significantly and positively correlated with the maximum torque applied to the femur specimens from NOR mice. The results for maximum torque, maximum shear stress, and torsional rigidity are similar to results found by previous researchers working with mouse femurs [14,15,20], indicating that the device design was effective. As mentioned by Brodt et al (1999), femoral length has been found to stop increasing at 20 weeks (140 days) of age, which means that values reported at approximately 70 days are recorded while the mouse femora are still growing. Table 3 summarizes results from several studies, including this study, for comparative purposes.

Possible sources of error in the experiment include bone specimen potting misalignment, chatter at the pinion gear and rack gear interface, unidentified bone specimen irregularities, alteration of bone mechanics due to exothermic properties of the PMMA cement, and the assumption of isotropy and homogeneity in some of the calculations performed. The most important factor that could contribute to error is the potting location of the bone. Torque calculations were performed under the assumption that the center of the proximal end of the femur was potted at a distance away from the rack gear interface that equaled the pitch radius of the pinion gear. It is highly unlikely that the bone specimens were potted exactly 11.902 millimeters from the interface; however, great care was taken to ensure that the specimens were potted as closely to the center of the potting tube as possible.

Conclusion

The torsional testing apparatus for murine long bones was found to be effective and accurate in measuring the mechanical properties of femora specimens from NOR mice. Results matched expected outcomes and values reported in previous studies. Future work will investigate differences between groups such as obese and non-obese mice, diabetic and non-diabetic mice, and standard DO-treated femora and hypoxic DO-treated femora.

Table 3. Comparison of Results between Studies on Torsional Loading of Mouse Femurs.

Study	Mouse Type	Specimen Age (days)	Specimen Length (mm)	Max Torque (N•mm)	Rotation Rate (degree/s)
This Study (2012)	Female NOR	73	14.29 ± 0.35	17.26 ± 1.37	1.0
Silva & Ulrich (2000)	Female C57BL/6	70	N/A	23.2 ± 4.2	1.0
Saunders et al (2010)	N/A	84	N/A	25.45 ± 4.0	1.1
Brodt et al (1999)	Female C57Bl/6	63	14.14 ± 0.31	21.0 ± 1.6	1.0

Acknowledgments

I would like to thank my research mentor, Dr. Alan Eberhardt, for his continued support of this research effort. He has provided invaluable feedback for the improvement of this project. Dr. Tim Nagy and Dr. Xingching Li in the Small Animal Bone Phenotyping Core at UAB generously allowed us to scan our specimens with the CT scanner in their lab. Joe Schwertz, a PhD student in the BME department, contributed significantly to the development of this project.

References

1. Doblaré, M., Garcia, J.M., and Gomez, M.J. (2004). Modeling bone tissue fracture and healing: a review. *Engineering Fracture Mechanics*, 71: 1809-1840.

2. Boskey, A. L., Wright, T. M. and van der Meulen, M. C. H. (2003), Guidelines for describing mouse skeletal phenotype. *Journal of Orthopaedic Research*, 21: 1–5.

3. Reddy GK, Stehno-Bittel L, Hamade S, Enwemeka CS. (2001). The biomechanical integrity of bone in experimental diabetes. *Diabetes Research and Clinical Practice*, 54: 1–8.

4. Cao, JJ. (2011). Effects of obesity on bone metabolism. *Journal of Orthopedic Surgery and Research*, 6: 30.

5. Janicka A, Wren TA, Sanchez MM, Dorey F, Kim PS, Mittelman SD, Gilsanz V. (2007). Fat mass is not beneficial to bone in adolescents and young adults. *The Journal of Clinical Endocrinology & Metabolism*, 92:143–147.

6. Thrailkill, KM, Liu, L, Wahl, EC, Bunn, RC, Perrien, DS, Cockrell, GE, Skinner, RA, Hogue, WR, Carver, AA, Fowlkes, JL, Aronson, J, and Lumpkinm CK. (2005). Bone formation is impaired in a model of type 1 diabetes. *Diabetes*, 54: 2875-2881.

7. Schwartz, AV. (2003). Diabetes mellitus: does it affect bone? *Calcified Tissue International,* 73:515–519

8. Beck TJ, Petit MA, Wu G, LeBoff MS, Cauley JA, and Chen, Z. (2009). Does obesity really make the femur stronger? BMD, geometry, and fracture incidence in the women's health initiative-observational study. *Journal of Bone And Mineral Research*, 24: 1369-1379.

9. Wohl GR, Loehrke L, Watkins BA, and Zernicke, RF. (1998). Effects of high-fat diet on mature bone mineral content, structure, and mechanical properties. *Calcified Tissue International,* 63: 74–79.

10. Núñez, N. P., Carpenter, C. L., Perkins, S. N., Berrigan, D., Jaque, S. V., Ingles, S. A., Bernstein, L., Forman, M. R., Barrett, J. C. and Hursting, S. D. (2007). Extreme obesity reduces bone mineral density: complementary evidence from mice and women. *Obesity,* 15: 1980–1987.

11. Wan, C., Shao, J., Gilbert, S.R., Riddle, R.C., Long, F., Johnson, R.S., Schipani, E., and Clemens, T.L. (2010). Role of HIF-1α in skeletal development. *Annals of the New York Academy of Sciences*, 1192: 322–326.

12. Vashishth, D., Tanner, K.E., and Bonfield, W. (2001). Fatigue of cortical bone under combined axial-torsional loading. *Journal of Orthopaedic Research*, 19: 414-420.

13. George, W.T. and Vashishth, D. (2005). Damage mechanisms and failure modes of cortical bone under components of physiological loading. *Journal of Orthopaedic Research*, 23: 1047-1053.

14. Nazarian, A., Entezari, V., Vartanians, V., Müller, R., and Snyder, B.D. (2009). An improved method to assess torsional properties of rodent long bones. *Journal of Biomechanics*, 42: 1720-1725.

15. Nazarian, A., Bauernschmitt, M., Eberle, C., Meier, D., Müller, R., and Snyder, B.D. (2008). Design and validation of a testing system to assess torsional cancellous bone failure in conjunction with time-lapsed micro-computed tomographic imaging. *Journal of Biomechanics*, 41: 3496–3501.

16. Silva, M.J., and Ulrich, S.R. (2000). In vitro sodium fluoride exposure decreases torsional and bending strength and increases ductility of mouse femora. *Journal of Biomechanics*, 33: 231-234.

17. Brodt, M.D., Ellis, C.B., and Silva, M.J. (1999). Growing C57B1/6 mice increase whole bone mechanical properties by increasing geometric and material properties. *Journal of Bone and Mineral Research*, 14: 2159-2166.

18. Saunders, M.M., Burger, R.B., Kalantari, B., Nichols, A.D., and Witman, C. (2010). Development of a cost-effective torsional unit for rodent long bone assessment. *Medical Engineering & Physics*, 32: 802-807.

Appendix

A1 - Calculations

1) Linear displacement for achieving a rotation rate of one degree per second:

$$s=r\theta$$

Where s is arc length, r is the gear pitch radius, and θ is the angle of twist. To find the rate of rotation:

$$\theta \doteq s/r$$

Where is the linear displacement rate of the rack gear and is the rate of rotation. To find the rate of linear displacement to match one degree of angular rotation per second, we will convert to radians per second:

$$(1 \text{ degree})/\text{second} \times (\pi \text{ radians})/(180 \text{ degrees}) = (0.0174 \text{ radians})/\text{second}$$

Solving for yields the following equation:

$$s \doteq r\theta \doteq (0.0174 \text{ radians/second})(11.906 \text{ mm}) = 0.2072 \text{ mm/second}$$

2) Weight force of the rack gear and connector.

Determining the weight of the rack gear and the connector part is essential to calculating the forces acting on the load cell.

$$F_{weight} = (m_{rack} + m_{connector})(g)$$

Where F_{weight} is the weight force of the rack gear and connector part in Newtons, m_{rack} is the mass of the rack gear, $m_{connector}$ is the mass of the connector part, and g is the acceleration due to gravity, which is 9.81 m/s^2.

The combined mass of the two parts was measured using a precision balance scale and was found to be 88.2 grams, or 0.0882 kilograms. The weight in Newtons can then be calculated:

$$F_{weight} = (0.0882 \text{ kg})(9.81) = 0.865 \text{ N}$$

A2 – Manufacturer Part Specifications

#	Part Name	Manufacturer/Vendor	Part Number	Material	Cost ($)
1	3” Rack Gear; 96 Pitch	Stock Drive Products/Sterling Instruments (SDP-SI)	S1810Y-RC-7A	2024-Al	62.76
2	Pinion Gear; 96 Pitch; 90 Teeth	Stock Drive Products/Sterling Instruments (SDP-SI)	S1063Z- 096A090	2024-Al	16.23
3	Block Housing; 0.375” ID	Stock Drive Products/Sterling Instruments (SDP-SI)	A 7Z28-P038	Sintered Al	4.86
4	Miniature Ball Bearing 0.1875” Bore Dia.	Spyraflow	PB0-SR3ZZ	Mounts: Al; Ball Bearings: Stainless Steel	11.64
5	Outside Rotating Tube	McMaster-Carr	89965K368	6061-Al	9.44
6	Inside Rotating Tube; 0.625” ID	McMaster-Carr	8978K163	6061-Al	6.14
7	Gearshaft	Smallparts.com (Amazon Supply)	B003U6I39G	6061-Al	5.29
				TOTAL	**116.36**